Efficient flexible polymer light emitting diodes with conducting polymer anodes†

J. Huang,[a] X. Wang,[a] A. J. deMello,[b] J. C. deMello*[b] and D. D. C. Bradley*[a]

Received 18th April 2007, Accepted 15th June 2007
First published as an Advance Article on the web 26th June 2007
DOI: 10.1039/b705918n

We report polymer light emitting diodes fabricated on flexible poly(ethyleneterephthalate) substrates coated with a layer of poly(3,4-ethylene-dioxythiophene) : poly(styrenesulfonate) that was lithographically patterned to define the anode structure. A blend of poly(9,9-dioctylfluorene-co-benzothiadiazole) and poly(9,9-dioctylfluorene-co-*N*-(4-butylphenyl)diphenylamine) was then spin-coated on top as the emissive layer and the device was completed by vacuum deposition of a LiF/Al bilayer cathode. The resulting yellow light emitting diodes had typical peak power and current efficiencies of 13.7 lm W^{-1} and 8.8 cd A^{-1} respectively, which compare well with values for similar devices fabricated on ITO-coated rigid glass substrates. A maximum luminance in excess of 7300 cd m^{-2} was achieved.

Colour displays based on organic light-emitting diodes (OLEDs) are being actively developed as an alternative to liquid crystal displays. The first generation of OLED displays are supported on rigid glass substrates, but there is considerable interest in using flexible plastic substrates (that for instance permit the use of roll-to-roll manufacturing techniques) to fabricate robust and conformable displays. OLEDs have, for example, been fabricated on poly(ethyleneterephthalate) (PET),[1–7] polycarbonate,[8] a poly(bis-cyclopentadiene) condensate,[9] poly(propylene adipate)[10] and polyimide.[11,12] The adoption of such materials presents a number of technological challenges including how to cope with their relatively poor thermal stability, a limitation that constrains their use to low-temperature processing routes. This has immediate implications for device fabrication since indium tin oxide (ITO; the dominant anode material for OLEDs) is typically deposited by thermal evaporation or sputtering at temperatures in excess of 350 °C, and even when deposited at lower temperature generally needs to be annealed in air or oxygen at those temperatures in order to achieve a suitably high conductivity. Methods of deposition on plastic substrates at lower temperatures are under development but to date they typically yield somewhat porous films with relatively low conductivity, limited optical transmission and degraded substrate adhesion, and lead ultimately to reduced device quality.[13] The use of a biased RF magnetron sputtering process may hold promise in this context.[10]

These issues, together with the tendency of ITO to crack when the substrate is flexed, have led researchers to seek alternative anode materials for flexible substrate applications. A variety of materials systems have been proposed including other metal oxides,[14] thin metallic films,[15] polymer–metal composites;[13] polymer–fullerene composites,[16] and conducting polymers.[1,17,18] Polymer based approaches are especially appealing because they allow deposition over large areas using techniques such as blade-coating, and planographic or inkjet printing, with obvious potential for reel-to-reel implementation. The two most widely used conducting polymers in this respect are polyaniline,[1] and poly(3,4-ethylenedioxythiophene) : poly(styrenesulfonate) (PEDOT : PSS).[17] Of these, PEDOT : PSS is the more common choice for display applications because polyaniline typically has a somewhat reduced transmission across the visible spectrum, with an absorption peak at 440 nm that prevents its use in full colour displays. PEDOT : PSS, on the other hand, has a high transparency across the whole visible spectral range which, together with its excellent hole-injecting properties,[19] has led to it being successfully utilised in a wide variety of OLEDs. It was, consequently, the material that we selected to use as the anode in our flexible substrate devices.

Our PET substrates were commercially sourced overhead projector sheets and the anode patterns were lithographically defined in 120 nm spin-coated layers of standard Baytron P[20]—a relatively high conductivity formulation of PEDOT : PSS from H. C. Starck GmbH. The Baytron P coated substrates were then spin-coated with an additional 40 nm layer of Baytron P VP AI4083—a lower conductivity formulation of PEDOT : PSS also supplied by H. C. Starck GmbH. This second layer is able to form a good contact with the active light-emitting polymer layer and we have generally found that its inclusion yields devices of substantially higher quality than those using the directly patterned Baytron P alone.[21] PET substrates with these two anode layers on top were next annealed at 120 °C for 20 minutes in a dry nitrogen atmosphere to remove trapped water, the presence of which can reduce the PEDOT : PSS conductivity.[22] Next, 90 nm emission layers, here comprising a 1 : 1 blend by weight of poly(9,9-dioctylfluorene-co-benzothiadiazole) (F8BT) and poly(9,9-dioctylfluorene-co-*N*-(4-butylphenyl)diphenylamine)

[a]*Experimental Solid State Physics Group, The Blackett Laboratory, Imperial College London, UK SW7 2AZ. E-mail: d.bradley@imperial.ac.uk*
[b]*Electronic Materials Group, Department of Chemistry, Imperial College London, UK SW7 2BZ. E-mail: j.demello@imperial.ac.uk*
† The HTML version of this article has been enhanced with colour images.

(TFB), were spin coated from 20 mg ml^{-1} xylene solution on top of the PEDOT : PSS. The resulting films were dried at 60 °C for two hours in a dry nitrogen atmosphere and finally a top contact comprising 1 nm of LiF capped with 100 nm of Al was thermally deposited though a shadow mask onto the polymer blend films *in vacuo* (2×10^6 Torr). The pixel area, defined by the overlap of the anode and cathode, was $\sim$1.5 mm^2. The schematic structure of our flexible LEDs is shown in the inset to Fig. 1. For comparison, devices of similar structure were fabricated using patterned ITO-coated glass in place of the Baytron P coated PET substrates. The remaining layers were the same as for the PET devices, namely: Baytron P VP AI4083 (60 nm)[23]/TFB : F8BT 1 : 1 blend (90 nm)/LiF (1 nm)/Al (100 nm). Electroluminescence (EL) spectra for the two device types were measured with a CCD spectrometer (Ocean Optics USB2000). The corresponding current–voltage characteristics were measured using a Keithley 2410 Source Measure Unit and the luminance was measured with a calibrated TOPCON Luminance Meter.

Fig. 1 shows the current density *vs.* voltage and luminance *vs.* voltage (*J–V–L*) characteristics for both the rigid glass and flexible PET substrate devices. The two devices have similar turn-on voltages of $\sim$1.9 V but the current density and luminance of the PET device are significantly lower than those of the glass substrate device, *e.g.* at 5 V $J_{PET}/J_{glass} \approx L_{PET}/L_{glass} \approx 10\%$, due to the higher conductivity of ITO compared to Baytron P, namely $\sim$2000 *versus* $\sim$5 S cm^{-1}.

The efficiency data for the two devices are shown in Fig. 2. Peak efficiencies of 13.7 lm W^{-1} and 8.8 cd A^{-1} were obtained

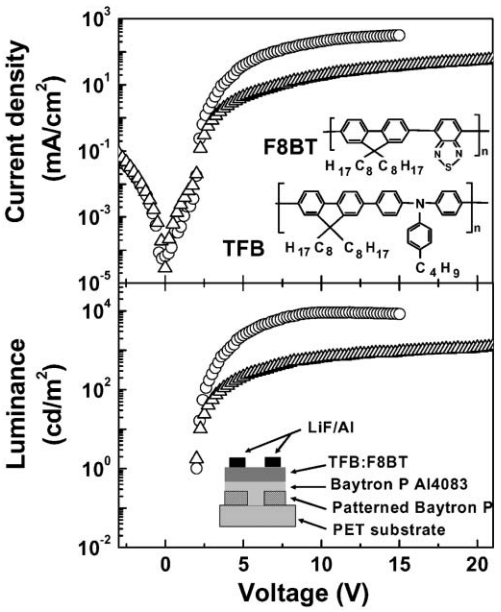

Fig. 1 Current density *vs.* voltage (upper panel) and luminance *vs.* voltage (lower panel) characteristics for rigid-substrate devices fabricated on ITO-coated glass (open circles) and flexible-substrate devices fabricated on Baytron P coated PET (open triangles). The device structures were [ITO/Baytron P AI4083/TFB : F8BT/LiF : Al] and [Baytron P/Baytron P AI4083/TFB : F8BT/LiF : Al] respectively. The upper panel insets show the F8BT and TFB chemical structures. The inset in the lower panel is a schematic of the PET-substrate device architecture.

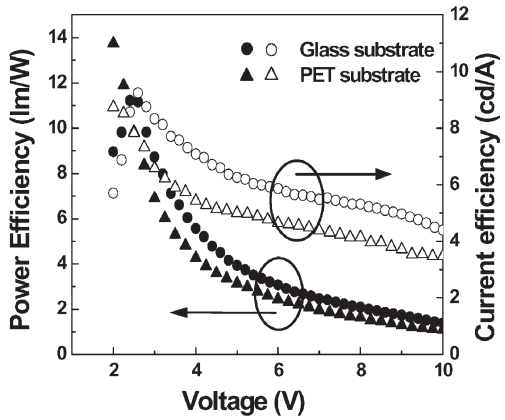

Fig. 2 The variation with applied voltage of the lm W^{-1} (filled symbols) and cd A^{-1} (open symbols) device efficiencies for the two devices shown in Fig. 1. Circles are for glass substrate devices and triangles for PET substrate devices.

for the PET substrate device, with efficiencies of 5.3 lm W^{-1} and 5.9 cd A^{-1} at 100 cd m^{-2}. These values compare with peak efficiencies of 11.2 lm W^{-1} and 9.2 cd A^{-1} for the glass substrate device, which were obtained at a brightness of 100 cd m^{-2}. The efficiencies of our PET devices compare very favourably with those reported for other flexible substrate devices.[18,24] For example, using *meso*-erythritol (1,2,3,4-tetrahydroxybutane) as an additive, Ouyang *et al.*[18] prepared PEDOT : PSS anodes with a conductivity 150 times higher than that of standard Baytron P. The efficiency of the resultant EL devices was 1.2 cd A^{-1} at 200 cd m^{-2}. We find 5.1 cd A^{-1} for our PET devices at the same luminance. Our results also compare reasonably well with current state of the art glass substrate devices. Importantly, the cd A^{-1} efficiency of our flexible substrate devices remains high (>4 cd A^{-1}) up to 8 V, at which voltage the luminance reaches $\sim$500 cd m^{-2}. The maximum luminance attainable with our flexible device was 7300 cd m^{-2}, although this required a high drive voltage of 80 V for reasons that are discussed below.

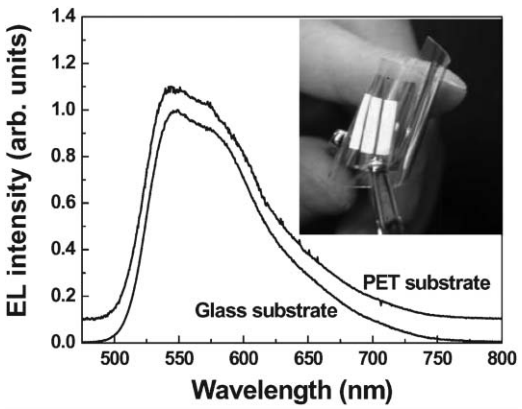

Fig. 3 Electroluminescence spectra for the two devices shown in Fig. 1. The PET substrate device spectrum (upper curve) has been vertically displaced for clarity. The CIE 1931 (*x*, *y*) coordinates for both devices are (0.455, 0.535). The inset shows a photograph of a flexed PET substrate device operating under ambient conditions (see the HTML version of this article for a colour version of this image).

Fig. 3 shows the electroluminescence spectra for the PET and glass substrate devices. No appreciable difference is apparent and the spectra are displaced vertically since otherwise they closely overlap. The inset to Fig. 3 shows an unencapsulated flexible substrate device with pixel size 2 mm × 8 mm working under ambient conditions. The device emits bright yellow light with CIE 1931 (x, y) coordinates (0.455, 0.535), and continues to function without any obvious problems when rolled up tightly (radius, $r_B < 4$ mm). This compares favourably with reports for ITO-coated flexible substrates, for which the anode resistance is found to increase sharply when $r_B < 8$ mm.[25]

As noted above, the higher resistance of the flexible device is directly attributable to the lower conductivity of PEDOT : PSS compared with ITO. The total device resistance, R, may be approximated as the sum of an axial (normal-to-plane) device resistance, R_{axial}, and an in-plane anode sheet resistance, $R_{in\text{-}plane}$. This latter resistance is relatively high for the flexible PET device. R_{axial} dominates below the turn-on voltage, even though the axial dimension of ~100 nm is very much smaller than the in-plane dimension of ~2 mm. Above turn-on, however, the rate of carrier injection into the active layer increases rapidly, leading to a sharp drop in R_{axial} and a total resistance that is more and more dominated by $R_{in\text{-}plane}$. A steadily increasing fraction of the applied bias is consequently dropped across the anode.

To investigate the influence of the sheet resistance on the device performance, an additional flexible device was fabricated in which the Baytron P anode was patterned in a u-shape as depicted in the plan-view schematic of Fig. 4. Contact was made to the PEDOT : PSS at two different locations, X and Y. In the first configuration (X), the in-plane distance to the region directly beneath the cathode was 1 mm. In the second configuration (Y), the in-plane distance was 37 mm and the influence of the sheet-resistance on the current–voltage characteristics was consequently stronger. The J–V characteristics for these two situations are shown in Fig. 5(a) (open symbols: squares for short anode length and circles for long)

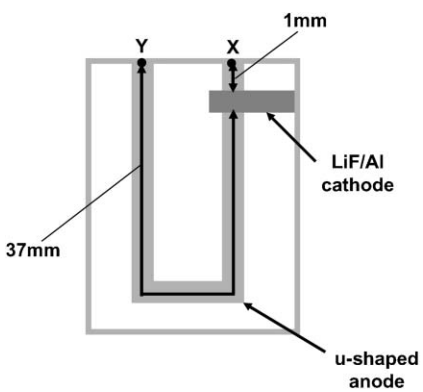

Fig. 4 Schematic showing an LED fabricated with a u-shaped PEDOT : PSS anode. Contact can be made to the anode at two different positions X and Y, resulting in respective in-plane distances of 1 and 37 mm from the point of contact to the region directly beneath the cathode. In the latter configuration, the current–voltage characteristics are more strongly influenced by the relatively high sheet resistance of the PEDOT : PSS anode.

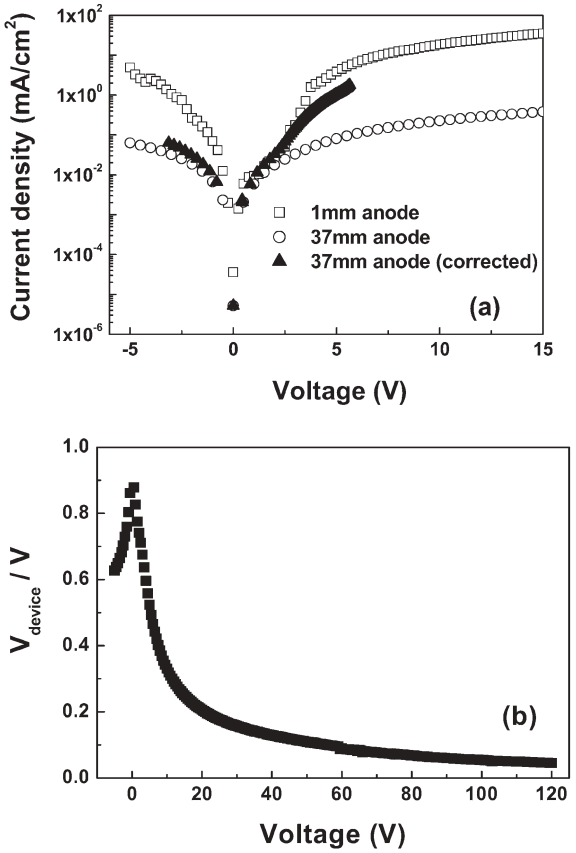

Fig. 5 (a) Current density (J) *vs.* voltage (V) characteristics for the device configurations illustrated in Fig. 4. The anode was in turn contacted at points X (1 mm anode length; open squares) and Y (37 mm anode length; open circles). The influence of the additional anode resistance when contacted at Y is apparent and results in a greatly reduced current density. The solid triangles data represent the J–V characteristics for the 37 mm anode length device after correction for the estimated voltage drop across the in-plane PEDOT : PSS sheet resistance (see text for details). (b) The calculated (see text for details) fractional voltage drop, V_{device}/V, across the emissive layer for the 37 mm anode length device as a function of applied voltage, V.

and the effect of the increased sheet resistance is obvious. An upper limit for the sheet resistance in the elongated-anode device configuration ($R_{in\text{-}plane}$ = 3.09 MΩ) can be estimated from the measured resistance at 120 V (for which the majority of the potential is dropped across $R_{in\text{-}plane}$). This resistance may in turn be used to deduce a lower limit for the potential, V_{device}, dropped across the device at lower biases: $V_{device} > V_{applied} - I \times R_{in\text{-}plane}$. The calculated lower limit for the fractional voltage drop, $V_{device}/V_{applied}$, across the elongated-anode device is shown in Fig. 5(b). For biases below 5 volts, over 50% of the applied voltage drops across the diode, whilst at 10 V only ~30% of the applied bias is dropped across the device. In this regime, the in-plane resistance of the anode presents a severe limitation for device power efficiency. Using the effective device voltages derived above, it is possible to correct the current–voltage characteristic for the elongated device. The resulting data (filled triangles) are also plotted in Fig. 5(a) and agree fairly well with the (uncorrected) data for the short-anode device configuration, indicating that the

decomposition of the total device resistance into additive in-plane and axial contributions is a reasonable first approximation. In passing, we note that the effects of sheet resistance can also be observed for ITO anodes, albeit at much higher currents due to the higher conductivity of ITO.[26]

In summary, we have reported the characteristics of flexible PET-substrate-based polymer LEDs with anodes comprising the conducting polymer PEDOT : PSS, without an underlying ITO layer. These devices with fluorene-based polymer blend emission layers give efficiencies of 5.3 lm W^{-1} and 5.9 cd A^{-1} at a luminance of 100 cd m^{-2}, values that compare favourably to other flexible devices reported in the literature and indeed to similar devices on ITO-coated glass substrates. The sheet resistance of the standard Baytron P formulation (as used here) is, however, rather too high and leads to a requirement for undesirably large drive voltages. Conversely it is well known that the conductivity of PEDOT : PSS films can be substantially enhanced by incorporating polyalcohols or high dielectric solvents into the PEDOT : PSS dispersion prior to deposition.[18,22,24] We therefore anticipate that improvements in device power efficiency should be achievable by further optimisation of the polymer anode properties. This is the focus of ongoing studies.

We would like to thank the Dow Chemical Company for providing the TFB and F8BT polymers used in this study. We also thank Sumation Co., Ltd for permission to publish this work: Sumation now holds the rights to the Lumation family of polyfluorenes and should be contacted for any future enquiries thereon. We additionally thank the UK Engineering and Physical Sciences Research Council (GR/R58949/01) for financial support.

References

1 G. Gustafsson, Y. Cao, G. M. Treacy, F. Klavetter, N. Colaneri and A. J. Heeger, *Nature*, 1992, **357**, 477.
2 G. Gustafsson, G. M. Treacy, Y. Cao, F. Klavetter, N. Colaneri and A. J. Heeger, *Synth. Met.*, 1993, **55–57**, 4123.
3 J. Ouyang, T. Guo, Y. Yang, H. Higuchi, M. Yoshioka and T. Nagatsuka, *Adv. Mater.*, 2002, **14**, 915.
4 T. Wang, C. Chen, S. Chang, Y. Tzeng and Y. Chao, *Microwave Opt. Technol. Lett.*, 2003, **38**, 406.
5 M. S. Weaver, L. A. Michalski, K. Rajan, M. A. Rothman, J. A. Silvernail, J. J. Brown, P. E. Burrows, G. L. Graff, M. E. Gross, P. M. Martin, M. Hall, E. Mast, C. Bonham, W. Bennett and M. Zumhoff, *Appl. Phys. Lett.*, 2002, **81**, 2929.
6 S. M. Chang, P. K. Su, G. J. Lin and T. J. Wang, *Synth. Met.*, 2003, **137**, 1025.
7 G. Gu, P. E. Burrows, S. Venkatesh, S. R. Forrest and M. E. Thompson, *Opt. Lett.*, 1997, **22**, 172.
8 W. F. Wu and B. S. Chiou, *Thin Solid Films*, 1997, **143**, 221.
9 Y. Hong, Z. He, N. S. Lennhoff, D. A. Banach and J. Kanicki, *J. Electron. Mater.*, 2004, **33**, 312.
10 Z. W. Yang, S. H. Han, T. L. Yang, L. Ye, D. H. Zhang, H. L. Ma and C. F. Cheng, *Appl. Surf. Sci.*, 2000, **161**, 279.
11 H. Kajii, T. Taneda and Y. Ohmori, *Thin Solid Films*, 2003, **438–439**, 334.
12 H. Lim, W. Cho, C. Ha, S. Ando, Y. Kim, C. Park and K. Lee, *Adv. Mater.*, 2002, **14**, 1275.
13 K. Yamada, K. Tamano, T. Mori, T. Mizutani and M. Sugiyama, *Proceedings of the 7th International Conference on Properties and Applications of Dielectric Materials* (Nagoya, Japan), IEEE, Piscataway, NJ, June 1–5, 2003, p. 49.
14 J. J. Ho, *Electron. Lett.*, 2003, **39**, 458.
15 J. Lewis, S. Grego, B. Chalamala, E. Vick and D. Temple, *Appl. Phys. Lett.*, 2004, **85**, 3450.
16 J. S. Moon, J. H. Park, T. Y. Lee, J. B. Yoo, C. Y. Park and J. M. Kim, *Sixth International Conference on the Science and Application of Nanotubes*, 2005, Sweden, Abstract P214.
17 A. N. Krasnov, *Appl. Phys. Lett.*, 2002, **80**, 3853.
18 J. Ouyang, C. Chu, F. Chen, Q. Xu and Y. Yang, *Adv. Funct. Mater.*, 2005, **15**, 203.
19 P. J. Brewer, P. A. Lane, J. Huang, A. J. deMello, D. D. C. Bradley and J. C. deMello, *Phys. Rev. B*, 2005, **71**, 205209.
20 J. Huang, R. Xia, Y. Kim, X. Wang, J. Dane, O. Hofmann, A. Mosley, A. J. de Mello, J. C. de Mello and D. D. C. Bradley, *J. Mater. Chem.*, 2007, **17**, 1043.
21 The conductivity of AI4083 is sufficiently low that cross-talk between adjacent pixels is not an appreciable problem and hence there is no need to pattern this second layer.
22 J. Huang, P. F. Miller, J. S. Wilson, A. J. deMello, J. C. de Mello and D. D. C. Bradley, *Adv. Funct. Mater.*, 2005, **2**, 290.
23 AI4083 spin-coats differently on ITO and Baytron P. The same solution and spin speed was used in each case resulting in a 60 nm film thickness on top of ITO compared to a 40 nm thickness on top of Baytron P.
24 W. H. Kim, A. J. Mäkinen, N. Nikolov, R. Shashidhar, H. Kim and Z. H. Kafafi, *Appl. Phys. Lett.*, 2002, **80**, 3844.
25 R. Paetzold, K. Heuser, D. Henseler, S. Roeger, G. Wittmann and A. Winnacker, *Appl. Phys. Lett.*, 2003, **82**, 3342.
26 X. Zhou, J. He, L. S. Liao, M. Lu, Z. H. Xiong, X. M. Ding, X. Y. Hou, F. G. Tao, C. E. Zhou and S. T. Lee, *Appl. Phys. Lett.*, 1999, **74**, 609.

